Pigeon-inspired optimization applied to constrained gliding trajectories

Article *in* Nonlinear Dynamics · December 2015

DOI: 10.1007/s11071-015-2277-9

2 authors, including:

Jiang Zhao
Beihang University (BUAA)
14 PUBLICATIONS **165** CITATIONS

SEE PROFILE

Nonlinear Dyn (2015) 82:1781–1795
DOI 10.1007/s11071-015-2277-9

ORIGINAL PAPER

Pigeon-inspired optimization applied to constrained gliding trajectories

Jiang Zhao · Rui Zhou

Received: 10 February 2015 / Accepted: 13 July 2015 / Published online: 24 July 2015

Abstract This paper presents the novel use of pigeon-inspired optimization (PIO) to generate the constrained gliding trajectory for hypersonic gliding vehicles. The velocity-dependent bank angle profile is developed in a quite simple formulation in order to reduce the searching space of the trajectory control command. The end-to-end trajectory and maximum-range trajectory are obtained by the enforced PIO algorithm which serves as an effective tool to deal with the typical path constraints and terminal conditions. Further, the forward and backward reversal logic is proposed to construct approximate footprints that can provide a fast decision in the mission deployment for nominal flights and abort situations. Numerical simulations demonstrate that the improved PIO algorithm is feasible and reliable to generate the constrained gliding trajectory for hypersonic gliding vehicles.

Keywords Pigeon-inspired optimization (PIO) · Constrained trajectory optimization · Gliding vehicles · Velocity-dependent bank angle · Forward and backward reversal logic

J. Zhao (✉) · R. Zhou
School of Automation Science and Electrical Engineering, Beihang University, Beijing 100191, China
e-mail: jzhao@buaa.edu.cn

1 Introduction

The global space transportation has spurred a great interest in hypersonic gliding vehicles for both civilian and military applications. The need for a reliable and efficient access to the space is promoting a rapid development of the gliding trajectory optimization and guidance techniques [1–4]. In the last decade, the progress has been witnessed by a series of experimental successes such as the DARPA's Falcon HTV, which demonstrates the great capability of flight inspection and data analysis [5].

The reference flight trajectory is a key component of the mission deployment for the reentry gliding vehicles [6]. Therefore, the reference trajectory design plays an important role in steering a reliable and safe reentry gliding flight. Generally, the reference trajectory is generated offline and preloaded on the gliding vehicle before its launching. Then, the gliding vehicle enters the atmosphere of the Earth at an altitude of about 80–100 km and the full gliding trajectory typically expands to the range of the terminal area an altitude of about 20–30 km [7–10]. It is a challenging task to design the reference trajectory for reentry gliding vehicles, because the three degree-of-freedom (3DOF) dynamics is highly nonlinear with limited control authority [11]. In addition, the gliding vehicle must subject to many path constraints in the complex environment such as the heating rate, dynamic pressure, and aerodynamic load [12–14].

In the current literature, three typical classes of approaches have been applied to the design of the

constrained gliding trajectory for the reentry gliding vehicles. The first type uses a reduced-order model to reduce the complexity of the optimal control problem [15]. Saraf et al. [16] presented the evolved acceleration guidance logic for entry (EAGLE) that consists of a trajectory planner to generate the atmospheric reentry gliding trajectory. Then, Leavitt et al. [17] made an extension of EAGLE to generate trajectories to most of the landing footprint, in which the feasible and optimal trajectories use the drag planning technique for the space shuttles. In addition, Guo et al. [18] obtained the drag acceleration-energy profile by using the interpolation between the upper and lower boundaries of the reentry corridor to generate the reentry gliding trajectory on board.

The second type employs the quasi-equilibrium glide phenomenon for lifting gliding vehicles. Shen et al. [19] proposed the quasi-equilibrium glide condition (QEGC) to generate the constrained gliding trajectory for reentry vehicles. The trajectory design is decomposed into two sequential one-parameter search problems. Then, Lu [20] presented a formal analysis to QEGC and obtained solutions in asymptotic expansions by a class of regular perturbation problems. On the basis of the QEGC, Ning et al. [21] also developed a new integrated guidance approach for reentry gliding vehicles which contains the online trajectory generator and guidance tracking controller. In addition, Xu et al. [22] employed the predictor-corrector principle and proposed an adaptive algorithm by means of QEGC to generate the gliding trajectory.

The third class of approaches adopts the direct trajectory optimization technique, in which the gliding trajectory design is performed by using pseudospectral methods. Zhao et al. [23] used the Gauss pseudospectral method to transcribe optimal control problem into the nonlinear programming problem by approximating the state and control at a set of discretization points. Then, Han et al. [24] proposed an hp-adaptive Radau pseudospectral method to generate the reentry gliding trajectory in order to increase the convergence rate as well as the computation accuracy. Guo et al. [25] employed a mapped Chebyshev pseudospectral method to the gliding trajectory optimization, in which a conformal map is applied to Chebyshev points to move the points closer to equidistant nodes. Further, Zhao et al. [26] developed a multistage trajectory control strategy based on the pseudospectral method including the trajectory estimation component and the trajectory refining component.

In this paper, the pigeon-inspired optimization (PIO) algorithm is used to generate the desired gliding trajectory for reentry gliding vehicles in a quite simple formulation. The goal of this paper was to present a new approach for solving a typical optimal control problem with a swarm intelligence method and avoiding the calculations required in common analytical approaches. This is accomplished by using an existing solution for a specific problem and then finding the simplified formulation to obtain other possible trajectories. The contribution of the paper is described as follows: (1) the basic PIO algorithm is enforced to deal with the equality and inequality constraints for typical trajectory optimization problem; (2) two kinds of the velocity-dependent bank angle profiles are developed to reduce the search space of the trajectory control command; and (3) a set of the reversed bank commands is generated by the forward and backward reversal logic in order to fast construct the approximate footprints. The paper is organized as follows. In Sect. 2, the trajectory dynamics and trajectory constraints of the reentry gliding vehicle are presented. In Sect. 3, the basic PIO algorithm and its improved version are introduced. Section 4 expatiates on the generation of the constrained gliding trajectory by using the improved PIO algorithm. The feasible applications of the proposed approach are demonstrated in Sect. 5. Finally, the concluding remarks are presented in Sect. 6.

2 Preliminary

2.1 Trajectory dynamics

The 3DOF point-mass dynamics of the reentry gliding vehicle over a spherical rotating Earth are given by the following equations of motion [6]

$$
\begin{aligned}
\dot{r} &= V\sin\gamma \\
\dot{\theta} &= \frac{V\cos\gamma\sin\psi}{r\cos\phi} \\
\dot{\phi} &= \frac{V\cos\gamma\cos\psi}{r} \\
\dot{V} &= -\frac{D}{m} - g\sin\gamma + \Omega^2 r(\sin\gamma\cos\phi \\
&\quad - \cos\gamma\sin\phi\sin\psi)\cos\phi \\
\dot{\gamma} &= \frac{L\cos\sigma}{mV} - \frac{g\cos\gamma}{V} + \frac{V\cos\gamma}{r}
\end{aligned}
$$

$$
\begin{aligned}
&+\frac{\Omega^2 r\cos\phi(\cos\gamma\cos\phi+\sin\psi\sin\phi\sin\gamma)}{V}\\
&+2\Omega\cos\phi\cos\psi\\
\dot{\psi}=&\frac{L\sin\sigma}{mV\cos\gamma}-\frac{V\cos\gamma\cos\psi\tan\phi}{r}\\
&-\frac{\Omega^2 r\sin\phi\cos\phi\cos\psi}{V\cos\gamma}\\
&+2\Omega(\tan\gamma\cos\phi\sin\psi-\sin\phi)
\end{aligned}
\tag{1}
$$

where r is the radial distance, θ and ϕ are the longitude and latitude, V is the Earth-relative velocity, γ and ψ are the flight-path angle and heading angle, σ is the bank angle, m is the mass of the vehicle, and Ω and g are the Earth angular velocity and gravitational acceleration. The aerodynamic drag force D and lift force L are described as

$$
\begin{aligned}
D&=\frac{1}{2}\rho V^2 C_D S_r\\
L&=\frac{1}{2}\rho V^2 C_L S_r
\end{aligned}
\tag{2}
$$

where S_r and ρ are the reference area and atmospheric density, respectively. The terms C_D and C_L are the drag and lift coefficients as functions of the angle of attack α and Mach number.

2.2 Trajectory constraints

The reentry gliding vehicles have allowable limits for maximum heating rate, dynamic pressure, and aerodynamic load. The typical constraint on the heating rate at the vehicle surface is given by [19]

$$
\dot{Q}=K_Q\rho^{0.5}V^{3.15}\le\dot{Q}_{\max}
\tag{3}
$$

where K_Q is a normalization constraint based on the heating model. The aerodynamic load is a hard constraint on the normal acceleration which is described as [19]

$$
n_{\mathrm{L}}=\sqrt{L^2+D^2}\big/mg_0\le n_{\mathrm{Lmax}}
\tag{4}
$$

where g_0 is the gravitational acceleration at the Earth surface. The dynamic pressure must also not exceed the limit of the vehicle's mechanical protection. It is constrained according to the following model as [19]

$$
q=\frac{1}{2}\rho V^2\le q_{\max}
\tag{5}
$$

In general, different terminal conditions are selected according to specified flight missions. The typical terminal conditions on the altitude, longitude, latitude, and velocity are given in terms of [6]

$$
r_f=r_f^*,\ \theta_f=\theta_f^*,\ \phi_f=\phi_f^*,\ V_f=V_f^*
\tag{6}
$$

where the subscript "f" denotes the terminal state and the superscript "*" represents the desired terminal states.

2.3 Problem formulation

Subject to the 3DOF equations of motion, the purpose of the gliding trajectory optimization is to find the control profiles such that the desired constrained gliding trajectories (e.g., the end-to-end trajectory and maximum-range trajectory) can be generated, meanwhile satisfying all the trajectory path constraints and trajectory terminal conditions. The gliding trajectory optimization for reentry vehicles is traditionally formulated as the optimal control problem in which the specific performance index is required. However, it is usually time-consuming to obtain an optimal gliding trajectory in the presence of numerous nonlinear equations of motion and nonlinear constraints. In this paper, we will simplify the control profiles so as to reduce the unknown parameters in the gliding trajectory optimization. The PIO algorithm is applied to design the constrained gliding trajectory by consideration in its simple structure and fast convergence rate. The suboptimal gliding trajectory and approximate footprint are generated by considering that a trade-off between the optimal solution and the complexity may improve the overall performance of gliding mission planning.

3 PIO algorithm with enforced constraints

The basic PIO algorithm and its improved version are introduced in this section. The PIO algorithm is one of the swarm intelligence methods that take the original inspiration from the natural phenomena [27]. It mimics the motion of a flock of pigeons when they find their home by using the magnetic field, the sun, and landmarks. As a population-based optimization tool, the PIO algorithm has a main strength that each pigeon uses the experience of the whole flock in the search

space rather than only the experience of its own. The PIO algorithm consists of two individual operators: (1) the map and compass operator; (2) the landmark operator [28]. To be specific, a flock of pigeons first shape the map by using the magnetic field and adjusting the direction according to the altitude of the sun. Then, they will fly close to the destination by using the landmarks neighboring them.

In the basic PIO, the population is described by N pigeons in total. The dimension of the problem to be solved is defined as n. Each pigeon in the flock represents a possible solution and corresponds to a specific value of the fitness function. The number of iterations in the PIO algorithm is N_{ITER}. The initial set of the pigeons is randomly selected in the searching space. The pigeon k is associated with a position vector $X(k)$ and a velocity vector $V(k)$ in the form of

$$X(k) = [x_1(k), x_2(k), \ldots, x_n(k)], \ (k = 1, 2, \ldots, N) \tag{7}$$

$$V(k) = [v_1(k), v_2(k), \ldots, v_n(k)], \ (k = 1, 2, \ldots, N) \tag{8}$$

In the map and compass operator, all the pigeons try to adjust and follow the best position in the flock. The position vector $X(k)$ and the velocity vector $V(k)$ are updated by the following equations [27]:

$$V^{(t)}(k) = V^{(t-1)}(k) \cdot \mathrm{e}^{-Rt} + rand \cdot \left(P^{(t-1)} - X^{(t-1)}(k)\right) \tag{9}$$

$$X^{(t)}(k) = X^{(t-1)}(k) + V^{(t)}(k) \tag{10}$$

where t is given iteration, R represents the map and compass factor that influences the velocity of each pigeon, $P^{(t-1)}$ denotes the best position in the pigeon flock, and *rand* is a random number within [0, 1].

In the landmark operator, half flock of the pigeons (they are away from the landmarks) is driven to follow the other half (they are close to the landmarks). The selected half of pigeons will guide the whole flock to the destination. The center of these pigeons can be obtained by [27]

$$C^{(t)} = \frac{\sum_{N_{\mathrm{P}}} X^{(t)}(k) \cdot fitness\left(X^{(t)}(k)\right)}{\sum fitness\left(X^{(t)}(k)\right)} \tag{11}$$

where *fitness* $(\cdot)$ reflects the objective function of the problem and N_{P} is the number of pigeons in the current iteration. As mentioned above, it is updated in the form of

$$N_{\mathrm{P}}^{(t)} = \frac{1}{2} N_{\mathrm{P}}^{(t-1)} \tag{12}$$

Thus, in this landmark operator, the position vector is manipulated by the following equation:

$$X^{(t)}(k) = X^{(t-1)}(k) + \mathrm{rand} \cdot \left(C^{(t)} - X^{(t-1)}(k)\right) \tag{13}$$

The basic PIO algorithm (7–13) has been proven to be a reliable tool to solve the flight-path planning problem [27,28]. However, it is difficult to deal with the gliding trajectory optimization problem that includes many path constraints and terminal conditions. Therefore, the basic PIO algorithm should be enforced and expand its further application to complex parameter optimization problem.

First, the components in each possible solution (i.e., the unknown parameters) in the PIO algorithm will be constrained in respective ranges. To be specific, the position component is bounded as follows:

$$a_i \le x_i^{(t)}(k) \le b_i, \quad (i = 1, 2, \ldots, n) \tag{14}$$

where a_i and b_i are given constants. The corresponding velocity vector should also be limited to suitable range; otherwise, the update of the map and compass operator would violate the constraint (14). It has the expression in the form of

$$-d_i \le v_i^{(t)}(k) \le d_i, \ d_i \triangleq b_i - a_i, \quad (i = 1, 2, \ldots, n) \tag{15}$$

Thus, the following rules are derived for the update laws (9–10), which can guarantee that the position vector $X(k)$ and the velocity vector $V(k)$ are constrained by (14–15)

(a) If $v_i^{(t)}(k) < -d_i \Rightarrow v_i^{(t)}(k) = -d_i$.
(b) If $v_i^{(t)}(k) > d_i \Rightarrow v_i^{(t)}(k) = d_i$.
(c) If $x_i^{(t)}(k) < a_i \Rightarrow x_i^{(t)}(k) = a_i$ and $v_i^{(t)}(k) = 0$.
(d) If $x_i^{(t)}(k) > b_i \Rightarrow x_i^{(t)}(k) = b_i$ and $v_i^{(t)}(k) = 0$.

Next, the equality and inequality constraints will be involved in the PIO algorithm in order to meet the requirement of gliding trajectory optimization. Taking

position vector $X(k)$ into consideration, the typical formulations of the equality and inequality constraints are described as

$$\varphi_p(X(k)) = 0, \quad (p = 1, 2, \ldots, m_p) \tag{16}$$

$$\lambda_q(X(k)) \leq 0, \quad (q = 1, 2, \ldots, m_q) \tag{17}$$

where m_p and m_q are the numbers of the equality and inequality constraints, respectively.

With regard to the equality constraints, many swarm intelligence methods use the popular solution by adding penalty terms to the fitness function. It is also employed in this paper. The fitness function consists of the basic objective function J_0 and the equality constraints (16) in the form of

$$fitness(X(k)) = J_{\min} = J_0 + \sum_{p=1}^{m} w_p \left|\varphi_p(X(k))\right| \tag{18}$$

where $w_p \geq 0$ are the weight coefficients. Note that the selection of the weights w_p depends on the actual parameter optimization problem.

With regard to the inequality constraints, the problem is less intractable, although they narrow the searching space of the feasible solutions. Since the inequality constraints do not decrease the degree of freedom of the optimization problem, a quite simple approach is used herein by setting the fitness function to an infinite value when some member in the pigeon flock violates any inequality constraint. To be specific, the following rule is derived to satisfy the constraint (17)

(e) If $\lambda_q(X(k)) > 0 \Rightarrow fitness(X(k)) = \infty$ and $V(k) = 0$.

In the rule above, the related velocity vector is also set to zero such that the flock of pigeons would not be affected by the velocity update when some inequality constraint is violated. The other generic steps of the iterations are similar to the basic PIO algorithm.

4 Gliding trajectory optimization

4.1 Outline

The trajectory control commands for reentry gliding vehicles consist of the angle of attack and the bank angle. Generally, the nominal angle of attack profile is applied to the design of gliding trajectory, because it is difficult for reentry gliding vehicles to adjust the angle of attack in full range. Therefore, the bank angle profile is typically enhanced for higher maneuverability and desired gliding trajectory.

In the following, the first part focuses on the design of the nominal angle of attack profile and the parameterized bank angle profile. Then, the 3DOF end-to-end trajectory and maximum-range trajectory are generated by using the PIO algorithm. At last, the forward and backward reversal logic is incorporated into the velocity-dependent bank angle profile to fast obtain the approximate landing footprint for reentry gliding vehicles.

4.2 Control profile design

The end-to-end mission planning from the reentry interface to the termination of the gliding phase is important to reentry gliding vehicles. Regarding a complete gliding trajectory, the angle of attack profile is usually determined by consideration in thermal protection, since the heating rate may reach the peak value at the beginning of the gliding phase. Herein, the nominal angle of attack profile is formulated as the monotonic function of the velocity

$$\alpha(V) = \begin{cases} \alpha_0, & V \geq V_\alpha \\ \alpha_0 - K_\alpha (V - V_\alpha)^2, & V < V_\alpha \end{cases} \tag{19}$$

where α_0 is the initial angle of attack, V_α is the specified critical velocity, and $K_\alpha > 0$ is a given constant. The typical illustration of the nominal angle of attack profile can be seen in Fig. 1.

In order to simplify the trajectory optimization problem, this part focuses on the design of the bank angle.

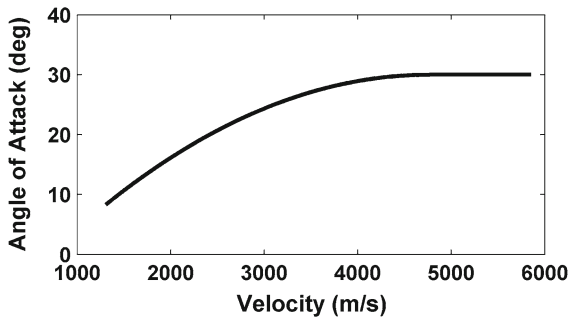

Fig. 1 Illustration of the nominal angle of attack profile

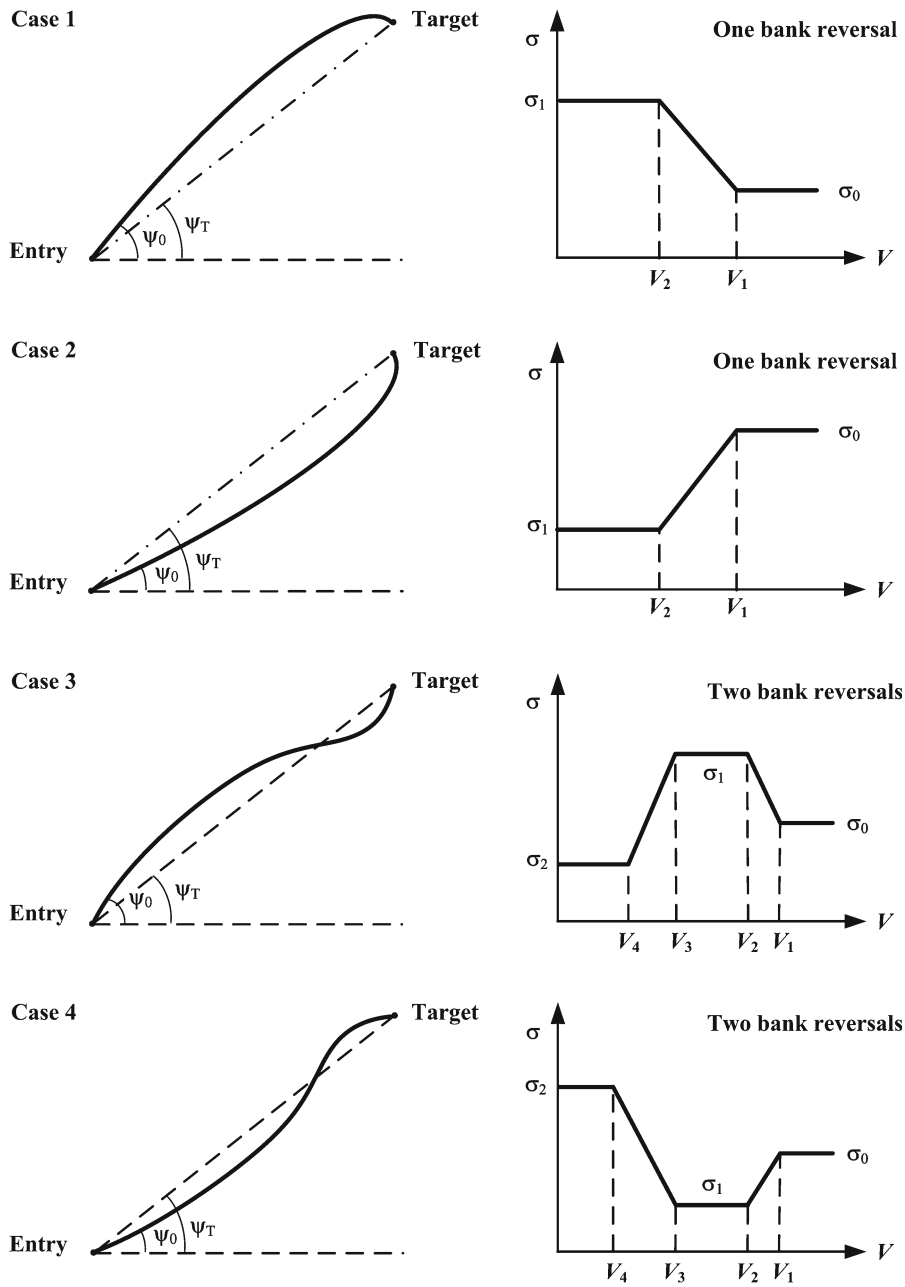

Fig. 2 Illustration of the velocity-dependent bank angle profiles

As shown in Fig. 2, the parameterized control profiles are developed to reduce the searching space of the optimal bank angle. The main idea is derived from the baseline bank reversal that is similar to the Apollo entry guidance. Two kinds of the velocity-dependent profiles are employed in quite simple forms like one bank reversal and two bank reversals. The formulation of the parameterized bank angle profiles is delineated in the following.

First, the expression of the velocity-dependent profiles with the shape of one bank reversal is given by the following equation:

$$\sigma(V)=\begin{cases}\sigma_0, & V>V_1\\ \sigma_0+\frac{V-V_1}{V_2-V_1}(\sigma_1-\sigma_0), & V_2<V\le V_1\\ \sigma_1, & V\le V_2\end{cases} \tag{20}$$

where V_1 and V_2 are the critical velocities, σ_0 is the initial bank angle, and σ_1 is the constant terminal bank angle. In detail, a constant bank angle σ_0 is used, during the initial descent phase, to integrate the 3DOF dynamics until the velocity decreases to V_1. To meet the requirement of the interface between gliding phase and terminal area energy management (TAEM), the terminal bank angle is set to be another constant value σ_1 as the critical velocity V_2 is reached. The bank angle profile is linear when the velocity stands between V_1 and V_2.

Further, additional rules are derived to specify the design of the bank angle profile according to the geometry of lateral gliding trajectory as shown in Fig. 2. Let $\Delta\psi$ represents the difference between the vehicle azimuth ψ_0 and the line-of-sight ψ_T from the vehicle to the target, the constant terminal bank angle in (20) can be determined by the following rules:

(f) If $\Delta\psi=\psi_0-\psi_T>0\Rightarrow\sigma_1>\sigma_0,\ \sigma_1>0$.
(g) If $\Delta\psi=\psi_0-\psi_T<0\Rightarrow\sigma_1<\sigma_0,\ \sigma_1<0$.

Similarly, the expression of the velocity-dependent profile with the shape of two bank reversals can be given by the following equation:

$$\sigma(V)=\begin{cases}\sigma_0, & V>V_1\\ \sigma_0+\frac{V-V_1}{V_2-V_1}(\sigma_1-\sigma_0), & V_2<V\le V_1\\ \sigma_1, & V_3<V\le V_2\\ \sigma_1+\frac{V-V_3}{V_4-V_3}(\sigma_2-\sigma_1), & V_4<V\le V_3\\ \sigma_2, & V\le V_4\end{cases} \tag{21}$$

where $V_1,\ V_2,\ V_3$ and V_4 are the critical velocities, σ_0 is the initial bank angle, and σ_1 and σ_2 are the constant bank angles to be determined. Then, considering the geometry of lateral gliding trajectory, rules can also be derived to design the parameterized bank angle profile:

(h) If $\Delta\psi=\psi_0-\psi_T>0\Rightarrow\sigma_1>\sigma_0,\ \sigma_1>0,\ \sigma_2<0$.
(i) If $\Delta\psi=\psi_0-\psi_T<0\Rightarrow\sigma_1<\sigma_0,\ \sigma_1<0,\ \sigma_2>0$.

Based on the above formulation, it is easy to obtain the optimal control profile as well as the desired gliding trajectory by searching the constant terminal bank angles and the critical velocities. Although the design of the velocity-dependent bank angle profile is different in approach from the baseline bank reversal, it is equally satisfactory in result.

4.3 Objective function and trajectory constraints

Assume that the nominal angle of attack profile and the initial bank angle are given in advance, the main goal of the optimization problem is to determine the parameters $(\sigma_1,\ V_1,\ V_2)$ in the profile (20) or the parameters $(\sigma_1,\sigma_2,\ V_1,\ V_2,\ V_3,\ V_4)$ in the profile (21). To meet the requirement of the 3DOF end-to-end gliding trajectory and maximum-range gliding trajectory, this part presents the formulation of the fitness function as well as guaranteed satisfaction of trajectory path constraints and terminal conditions.

As mentioned in the previous section, both the objective function and the equality constraints can be generally incorporated into the fitness function. Therefore, the trajectory terminal conditions (6), which are in the basic form of equality constraints, can be solved by adding penalty terms to the fitness function. With regard to the end-to-end gliding trajectory, the fitness function that consists of the objective function and terminal constraints has the typical expression as

$$\begin{aligned}fitness\,(X(k))=J_{\min}=J_0&+w_1\left|r_f-r_f^*\right|\\&+w_2\left|V_f-V_f^*\right|+w_3\left|\theta_f-\theta_f^*\right|\\&+w_4\left|\phi_f-\phi_f^*\right|\end{aligned} \tag{22}$$

where $w_p\ge 0\,(p=1,2,3,4)$ are the weight factors related to the trajectory terminal conditions (6). The selection of the objective function J_0 usually depends on specified requirement such as minimum total heat load. In the same way, the following fitness function can be obtained to generate the maximum-range gliding trajectory

$$\begin{aligned}fitness\,(X(k))=J_{\min}=\frac{1}{S_f}&+w_1\left|r_f-r_f^*\right|\\&+w_2\left|V_f-V_f^*\right|\end{aligned} \tag{23}$$

where S_f represents the terminal crossrange of the constrained gliding trajectory.

Table 1 Pseudocode of the proposed algorithm

1:	**//Initialization**
2:	Set the parameters of the algorithm: n, N, N_{ITER}, R, a_i, b_i
3:	Set the initial states of the vehicle: (r_0, θ_0, ϕ_0, V_0, γ_0, ψ_0)
4:	Choose the unknown parameters: (σ_1, V_1, V_2) or (σ_1, σ_2, V_1, V_2, V_3, V_4)
5:	Generate N random pigeons and initial the position vector $X(k)$ and velocity vector $V(k)$
6:	Formulate the fitness function using (22) or (23)
7:	**//Main loop**
8:	**while** iteration $t \leq N_{\mathrm{ITER}}$ (stop criteria) **do**
9:	**//The map and compass operator**
10:	**for** N pigeons **do**
11:	Update pigeon velocity using (9)
12:	Update pigeon position using (10)
13:	Evaluate the fitness and determine the current best position
14:	**end for**
15:	**//The landmark operator**
16:	Rank the fitness and select the half flock of pigeons close to the landmarks
16:	Determine the center of the selected half using (11) and (12)
17:	Update pigeon position using (13)
19:	**end while**
20:	**//Results**
21:	Find the global best position, i.e., the optimal solution
22:	Determine the trajectory control profile using (20) or (21)
23:	Generate the gliding trajectory and validate the path constraints

With regard to the trajectory path constraints (3–5), the common solution is to transform them into the boundary limits of bank angle profile. Herein, the constrained PIO algorithm provides an easier approach to enforce deal with these inequality constraints. According to the rule (e), if one of the path constraints (3–5) is violated by individual pigeon, the PIO algorithm will simply set the fitness function to be an infinite value and stop the velocity update. The search space of the position vector is reduced to meet the trajectory path constraints. Thus, the complete pseudocode of the proposed optimization algorithm can be listed in Table 1.

In fact, the objective of this paper was to present a new method for solving the gliding trajectory optimization problem and avoiding the calculations needed in common analytical approaches. This is accomplished by using the improved PIO algorithm with simplified bank profile design. Indeed, the problem can be solved by various optimization methods such as the classical method of descent. The swarm intelligence may not have better performance in computational complexity than the classical methods because the computation time is also influenced by the swarm size and the designated iterations. However, the swarm intelligence may possibly obtain a global optimal solution without a rigorous initial guess of the unknown parameters. For this reason, the improved PIO algorithm is selected for the gliding trajectory optimization problem.

4.4 Footprint generation

The footprint for the gliding vehicle provides the critical information of reachable locations with the TAEM interface. Assume that the maneuverability of the gliding vehicle is uniform, and then, the region of the footprint mainly depends on the initial reentry states, control boundaries, path constraints, and terminal conditions [2]. In detail, the footprint is a two-dimensional set determined by the longitude and latitude, for which the terminal altitude and velocity should be constrained to the desired values. As shown in Fig. 3, two kinds of shapes are typically used to describe the footprint. One is like a fan and the other like a polygon.

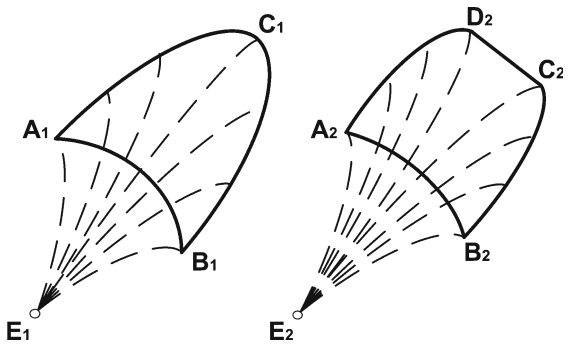

Fig. 3 Illustration of typical footprints

In general, the footprint computation problem is solved by searching a series of maximum-crossrange trajectories that have different downrange [29]. In addition, the direct trajectory optimization technique can be employed to generate the footprints by using the pseudospectral method [30]. However, it is quite time-consuming to obtain an accurate footprint and also complex to formulate the optimization problem in the mission deployment for both nominal flights and abort situations. Therefore, a simple approach to generate the approximate footprint is required which may provide a feasible solution for a fast decision of the landing options.

As shown in Fig. 4, the velocity-dependent bank angle profile is used herein to present the basic idea of the forward and backward reversal logic. To be specific, the forward reversal criterion is that the sign of the bank angle profile turns reversed after the velocity decreases to the critical value. The magnitude remains unchanged. The logic can be formulated by the following equation:

$$\sigma_{\mathrm{cmd}}(V) = \begin{cases} \sigma_{\mathrm{cmd}}(V), & V \geq V_+ \\ -\sigma_{\mathrm{cmd}}(V), & V < V_+ \end{cases} \tag{24}$$

where $\sigma_{\mathrm{cmd}}(V)$ is the selected bank angle profile and V_+ is the critical velocity in the forward reversal logic.

Table 2 Initial states of the gliding vehicle (Example 1)

h (km)	V (m/s)	θ (deg)	ϕ (deg)	γ (deg)	ψ (deg)
75.0	6000.0	0.0	0.0	−1.0	60.0

In contrast, the backward reversal turns the sign of the bank angle reversed before the velocity decreases to the critical value. The expression of the backward reversal logic is given by

$$\sigma_{\mathrm{cmd}}(V) = \begin{cases} -\sigma_{\mathrm{cmd}}(V), & V \geq V_- \\ \sigma_{\mathrm{cmd}}(V), & V < V_- \end{cases} \tag{25}$$

where V_- is the critical velocity in the backward reversal logic.

Thus, the main process of the footprint generation can be described as follows. First, the gliding trajectory with the maximum crossrange is obtained by constrained PIO algorithm that is presented in the previous section. Then, the optimal bank angle profile is used to generate the reversed bank command set by selecting different critical velocities V_+ and V_-. And further, the 3DOF dynamics are numerically integrated by the reversed bank commands such that the approximate footprint consists of a group of gliding trajectories with different crossrange. Note that the reversed bank command set depends on the same interval of velocity, and therefore, these gliding trajectories will end at the specified terminal velocity. In addition, the forward and backward reversal logic does not change the magnitude of the velocity-dependent bank angle profile such that the terminal constraint on the altitude would not be violated.

5 Numerical simulations

In this section, the numerical results of the gliding trajectory generation are presented by using the con-

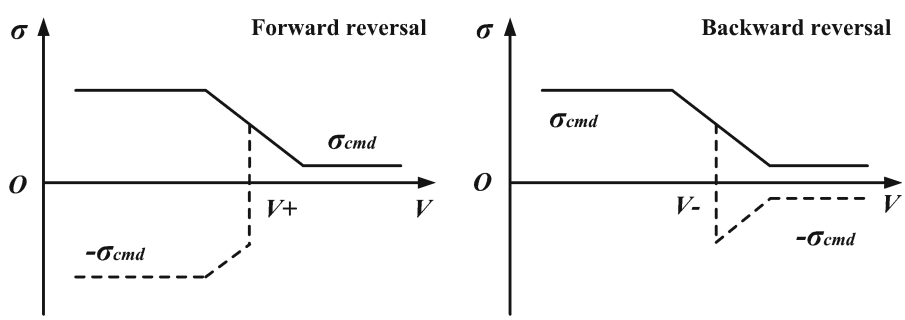

Fig. 4 Illustration of the forward and backward reversal logic

Table 3 PSO and PIO results of the best fitness and parameters in 10 runs

Algorithms	Best fitness	Best parameters			Mean
		σ_1 (deg)	V_1 (m/s)	V_2 (m/s)	
PSO	0.0371	49.145	5336.7	4055.4	0.0453
PIO	0.0365	47.865	5571.9	4251.7	0.0437

strained PIO algorithm. The total number of the pigeons is set to $N = 60$. The maximum number of the iterations is set to $N_{\mathrm{ITER}} = 40$. The factor of the map and compass operator is $R = 0.2$. The aerodynamic and characteristics parameters use the CAV-H data [31]. The nominal angle of attack profile is determined by the following parameters: $\alpha_0 = 30°$, $K_\alpha = 0.21$, $V_\alpha = 4764.2$ m/s (i.e., 14 Mach). The initial value of the bank angle profile is set to $\sigma_0 = 0°$. The limits of the bank angle boundary is set to $\sigma_{\max} = 60°$ and $\sigma_{\min} = -60°$. The path constraints remain fixed throughout the simulations as $Q_{\max} = 0.8$ MW/m^2, $q_{\max} = 80$ kPa, and $n_{\mathrm{Lmax}} = 4$.

5.1 Example 1 (maximum-range gliding trajectory)

This example presents the generation of the maximum-range gliding trajectory based on the design of the velocity-dependent bank angle profile. Herein, the parameterized profile (20) is used for the trajectory control input. The initial states of the reentry gliding vehicle are listed in Table 2. The terminal trajectory conditions are set to be $h = 24$ km and $V = 1500$ m/s, respectively. The objective function (23) is selected to obtain the gliding trajectory with maximum crossrange.

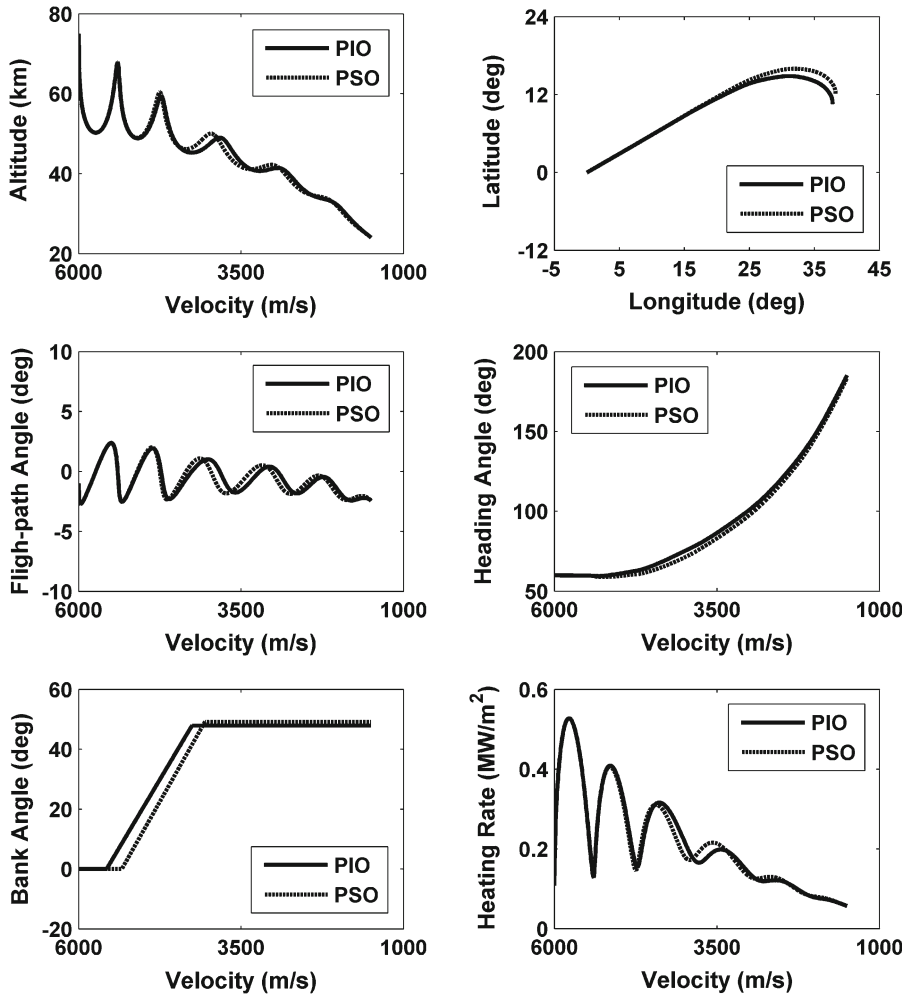

Fig. 5 Maximum-range gliding trajectories

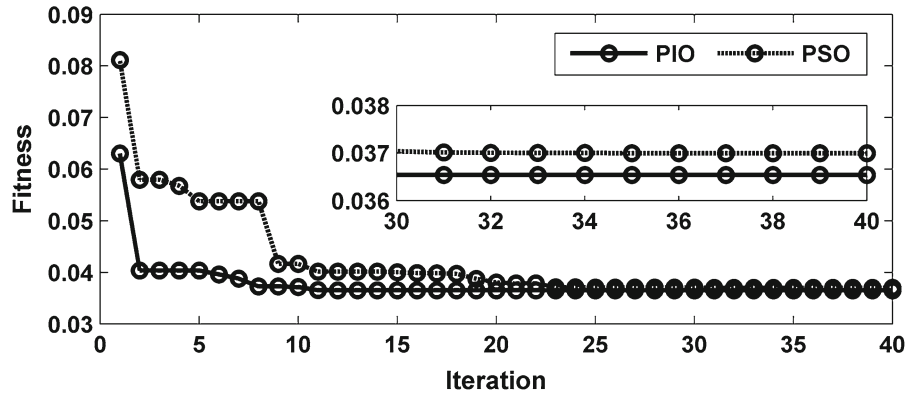

Fig. 6 Comparative evolution curves of the best fitness

Table 4 Initial states of the gliding vehicle (Example 2)

Cases	h (km)	V (m/s)	θ (deg)	ϕ (deg)	γ (deg)	ψ (deg)	Reversals
PIO 1	69.0	5850.0	10.0	0.0	−1.0	53.0	One
PIO 2	68.5	5800.0	5.0	10.0	−1.0	65.0	One
PIO 3	68.0	5750.0	30.0	−10.0	−1.0	33.0	One
PIO 4	69.5	5900.0	0.0	20.0	−1.0	80.0	Two
PIO 5	67.5	5800.0	20.0	−5.0	−1.0	47.0	Two

Table 5 PIO results of the fitness and parameters in the five cases

Cases	Fitness	Parameters					
		σ_1 (deg)	σ_2 (deg)	V_1 (m/s)	V_2 (m/s)	V_3 (m/s)	V_4 (m/s)
PIO 1	0.0165	6.632	–	4499.8	2808.0	–	–
PIO 2	0.0222	19.472	–	4698.3	2507.7	–	–
PIO 3	0.0186	−18.742	–	5049.1	2524.5	–	–
PIO 4	0.0233	31.495	−27.872	5113.3	4399.0	3382.7	2273.8
PIO 5	0.0236	−21.883	23.723	5002.5	4291.1	3400.4	1476.3

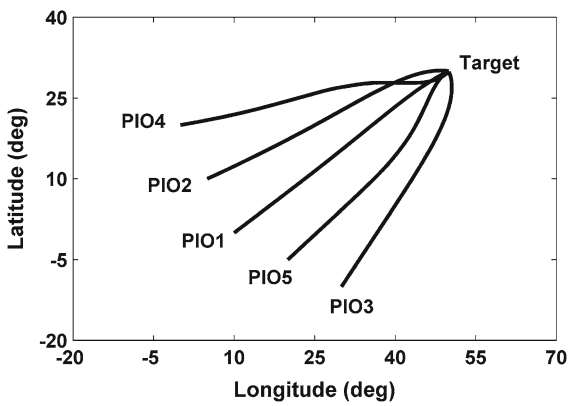

Fig. 7 Results of the ground tracks

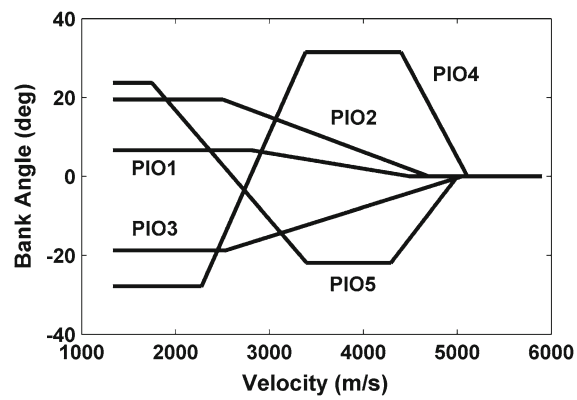

Fig. 8 Results of the bank angle profiles

Table 3 shows the PIO results of the best fitness values and parameters in comparison with the PSO algorithm. It can be found that the PIO and PSO obtain similar solutions in the best fitness value. However, the PIO algorithm has the better result with lower mean fitness value in 10 runs. Figure 5 illustrates the maximum-

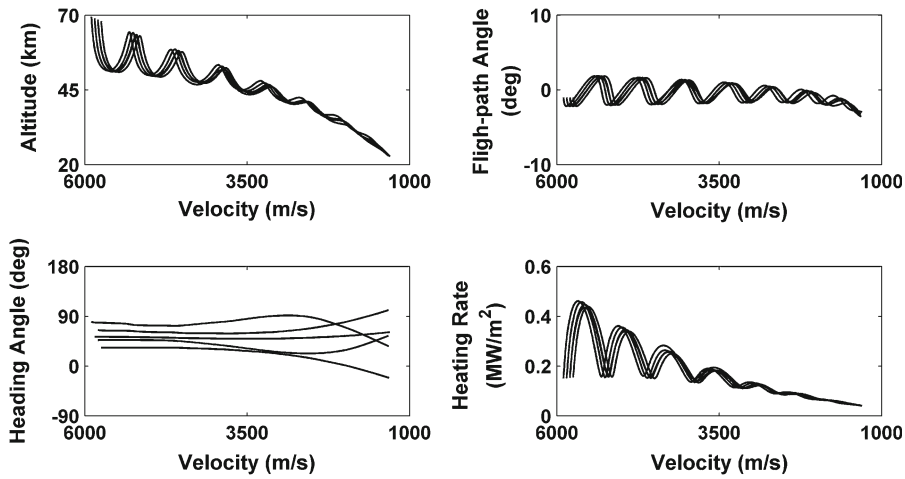

Fig. 9 End-to-end gliding trajectories

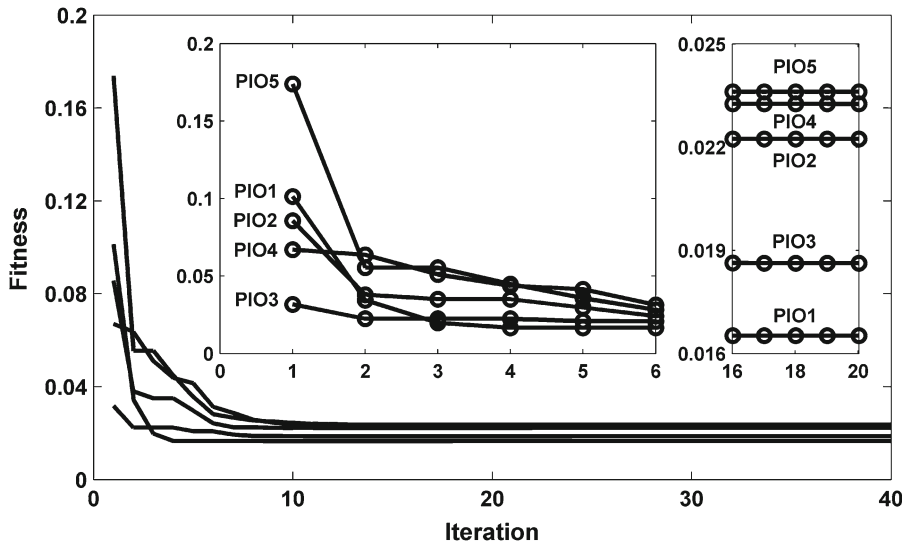

Fig. 10 Evolution curves of the fitness in the five cases

range gliding trajectories including the state, control, and path constraints. The PIO and PSO results are represented by the solid line and dot line, respectively. The histories of the altitude–velocity profiles show that the terminal trajectory conditions are satisfied with high accuracy. The flight-path angles remain to be small magnitude around zero which shows the common characteristic of the reentry gliding vehicle. The similar bank angle profiles are obtained by the PIO and PSO algorithms. The solutions of the unknown parameters in the control profiles are listed in Table 3. Figure 6 presents the trend of the fitness functions over 40 iterations. It is seen that both the fitness values in the PIO and PSO reach a convergence within the given number of iterations. However, the PIO algorithm has a much faster convergence rate than the PSO algorithm. Note that the suboptimal solutions are obtained herein because the bank angle profile is parameterized. In addition, a trade-off between the total number of pigeons and the optimal solution will notably improve the computational efficiency.

5.2 Example 2 (end-to-end gliding trajectory)

Based on the constrained PIO algorithm, five end-to-end gliding trajectories are generated in this simulation with the same target at $\theta_f = 50°$ and $\phi_f = 30°$. Herein, the velocity-dependent bank angle profile (20) is applied to the first three end-to-end missions and the two other missions employ the bank angle profile (21). Table 4 lists the initial states of the reentry glid-

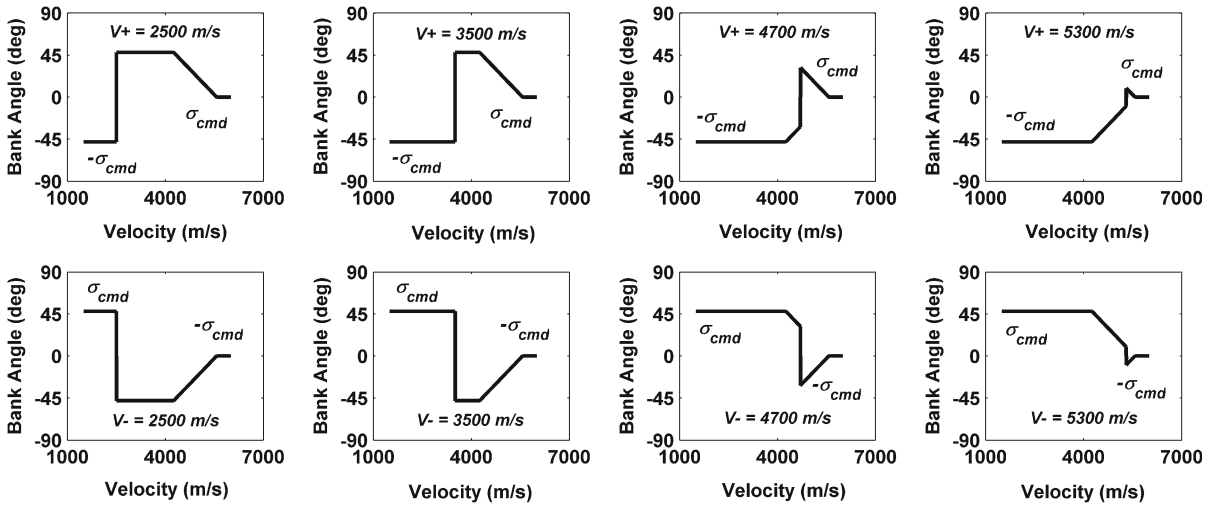

Fig. 11 Samples of the reversed bank commands

ing vehicle in detail. The terminal trajectory conditions are set to $h = 23$ km and $V = 1300$ m/s, respectively. The objective function (22) is selected to obtain the end-to-end gliding trajectory. The results of the fitness value and the parameters for the five cases are listed in Table 5.

The ground tracks are plotted in Fig. 7. It can be seen that the reentry gliding vehicle can be driven to the specified target although different initial reentry states are given in the example. All the ground tracks in the five cases are smooth enough and show that the velocity-dependent bank angle profiles (20) and (21) are reliable to generate the end-to-end gliding trajectory. Figure 8 presents the control profiles in detail, from which we can find that the solutions of the critical velocity and terminal bank angle agree with the geometry of the end-to-end gliding trajectories. The histories of the altitude, flight-path angle, heading angle, and path constraint are illustrated in Fig. 9. It is demonstrated that the PIO algorithm is feasible to deal with the typical equality constraints and inequality constraints in the trajectory optimization problem. In addition, Fig. 10 presents that the evolution curves of the fitness in the five cases converge fast to respective values within the maximum number of iterations, which shows an efficient application of the constrained PIO algorithm to generate the end-to-end gliding trajectory. It can also be found that the first three cases (PIO 1, PIO 2 and PIO 3) have lower fitness values than the two other cases (PIO 4 and PIO 5), which demonstrates that the velocity-dependent bank angle profile (20) results in better solutions than the bank angle profile (21).

5.3 Example 3 (Footprints)

In this part, the generation of the approximate footprint is performed by using the forward reversal logic (24) and the backward reversal logic (25). Herein, the PIO solution of the optimal bank angle profile obtained in Example 1 will be used to generate two sets of the reversed bank commands. The initial states of the gliding vehicle as well as the terminal trajectory conditions for the TAEM interface are the same as those in Example 1.

Figure 11 presents some typical samples of reversed bank commands formulated by using the forward and backward reversal logic with different critical velocities V_+ and V_-. It can be seen that by selecting a specific critical velocity, a pair of the forward and backward reversed bank commands are constructed symmetrically. The results also show that both the velocity interval and the magnitude of the bank angle profile remain unchanged. Based on the reversed bank commands, two sets of the gliding trajectories can be fast generated by integrating the 3DOF equation of motion. Then, two approximate footprints are constructed by these gliding trajectories with different crossrange as shown in Fig. 12. The corresponding gliding trajectories that are derived by the above samples of reversed bank commands are marked in the footprints. The approximate

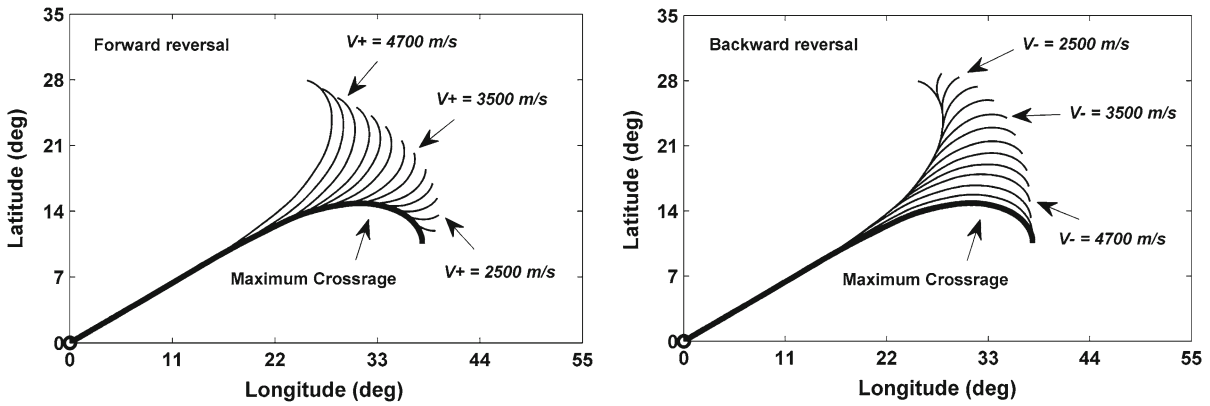

Fig. 12 Illustration of the approximate footprints

footprints may provide effective decision of the landing options in mission deployment for both nominal flights and abort situations.

6 Conclusions

The simplified design of the control profiles may contribute to enhance the flexibility of gliding trajectory optimization. In this paper, the standardized bank angle profiles are developed in a quite simple form to reduce the searching space of the trajectory control command. Based on these velocity-dependent bank angle profiles, the end-to-end and maximum-range gliding trajectories for the reentry vehicle are generated by using the constrained PIO algorithm. The simulation results demonstrate that the improved PIO algorithm is an effective tool to deal with the trajectory path constraints by setting the fitness function to an infinite value if some pigeon in the flock violates these inequality constraints. The trajectory terminal conditions can also be solved by adding penalty terms to the fitness function. In addition, the forward and backward reversal logic is proposed to generate a set of reversed bank commands, by which the two-dimensional footprints can be fast constructed. Although the footprints are obtained approximately, they may provide feasible solutions for fast determination of the landing options in both nominal flights and abort situations. The future work will focus on the design of the closed-loop guidance law and test the ability of the trajectory control with dispersions and uncertainties in the complex environment.

Acknowledgments The authors would like to thank the editors and reviewers for their critical review of this manuscript. This study was supported by National Natural Science Foundation of China (Nos: 61273349, 61203223).

References

1. Zong, Q., Wang, F., Tian, B., Rui, R.: Robust adaptive dynamic surface control design for a flexible air-breathing hypersonic vehicle with input constraints and uncertainty. Nonlinear Dyn. **78**(1), 289–315 (2014)
2. Zhao, J., Zhou, R., Jin, X.: Progress in reentry trajectory planning for hypersonic vehicle. J. Syst. Eng. Electron. **25**(4), 627–639 (2014)
3. Sun, H., Li, S., Sun, C.: Finite time integral sliding mode control of hypersonic vehicles. Nonlinear Dyn. **73**(1–2), 229–244 (2014)
4. Zhao, J., Zhou, R.: Unified approach to cooperative guidance laws against stationary and maneuvering targets. Nonlinear Dyn. doi:10.1007/s11071-015-2096-z
5. Yan, X., Lyu, S., Tang, S.: Analysis of optimal initial glide conditions for hypersonic glide vehicles. Chin. J. Aeronaut. **27**(2), 217–225 (2014)
6. Zhao, J., Zhou, R.: Reentry trajectory optimization for hypersonic vehicle satisfying complex constraints. Chin. J. Aeronaut. **26**(6), 1544–1553 (2013)
7. Xu, B., Wang, D., Sun, F., Shi, R.: Direct neural discrete control of hypersonic flight vehicle. Nonlinear Dyn. **70**(1), 269–278 (2012)
8. Lu, Y., Huang, G., Nan, Y.: A survey of numerical algorithms for trajectory optimization of flight vehicles. Sci. China Technol. Sci. **55**(9), 2538–2560 (2012)
9. Tian, B., Fan, W., Zong, Q.: Integrated guidance and control for reusable launch vehicle in reentry phase. Nonlinear Dyn. **80**(1–2), 397–412 (2015)
10. Zhao, J., Zhou, R., Zhang, C.: Predictor-corrector reentry guidance satisfying no-fly zone constraints. Acta Armamentarii **36**(5), 823–830 (2015)
11. Gao, G., Wang, J.: Observer-based fault-tolerant control for an air-breathing hypersonic vehicle model. Nonlinear Dyn. **76**(1), 409–430 (2014)

12. Zhao, J., Zhou, R.: Particle swarm optimization applied to hypersonic reentry trajectories. Chin. J. Aeronaut. **28**(3), 822–831 (2015)
13. Xie, Y., Liu, H., Tang, G., Zheng, W.: Highly constrained entry trajectory generation. Acta Astronaut. **88**(1), 44–60 (2013)
14. Zhao, J., Zhou, R., Zhang, C.: Predictor-corrector reentry guidance satisfying no-fly zone constraints. J. Beijing Univ. Aeronaut. Astronaut. **41**(5), 864–870 (2015)
15. Mease, K.D., Chen, D.T., Teufel, P., et al.: Reduced-order entry trajectory planning for acceleration guidance. J. Guid. Control Dyn. **25**(2), 257–266 (2002)
16. Saraf, A., Chen, D.T., Leavitt, J.A., et al.: Design and evaluation of an acceleration guidance algorithm for entry. J. Spacecr. Rockets **41**(6), 986–996 (2004)
17. Leavitt, J.A., Mease, K.D.: Feasible trajectory generation for atmospheric entry guidance. J. Guid. Control Dyn. **30**(2), 473–481 (2007)
18. Guo, J., Fu, Y., Cui, N.: Three dimensional autonomous entry guidance method. Control Decis. **28**(5), 688–695 (2003)
19. Shen, Z., Lu, P.: Onboard generation of three dimensional constrained entry trajectories. J. Guid. Control Dyn. **26**(1), 111–121 (2003)
20. Lu, P.: Asymptotic analysis of quasi-equilibrium glide in lifting entry flight. J. Guid. Control Dyn. **29**(3), 662–670 (2006)
21. Ning, G., Zhang, S., Fang, Z.: Integrated entry guidance for reusable launch vehicle. Chin. J. Aeronaut. **20**(1), 1–8 (2007)
22. Xu, M., Chen, K., Liu, L., Tang, G.: Quasi-equilibrium glide adaptive guidance for hypersonic vehicles. Sci. China Technol. Sci. **55**(3), 856–866 (2012)
23. Zhao, J., Zhou, R., Jin, X.: Gauss pseudospectral method applied to multi-objective spacecraft trajectory optimization. J. Comput. Theor. Nanosci. **11**(10), 2242–2246 (2014)
24. Han, P., Shan, J., Meng, X.: Re-entry trajectory optimization using an hp-adaptive Radau pseudospectral method. Proc. Inst. Mech. Eng. Part G J. Aerosp. Eng. **227**(10), 1623–1636 (2013)
25. Guo, X., Zhu, M.: Direct trajectory optimization based on a mapped Chebyshev pseudospectral method. Chin. J. Aeronaut. **26**(2), 401–412 (2013)
26. Zhao, J., Zhou, R., Jin, X.: Reentry trajectory optimization based on a multistage pseudospectral method. ScientificWorldJournal **878193**, 1–13 (2014). doi:10.1155/2014/878193
27. Duan, H., Qiao, P.: Pigeon-inspired optimization: a new swarm intelligence optimizer for air robot path planning. Int. J. Intell. Comput. Cybern. **26**(2), 401–412 (2013)
28. Zhang, B., Duan, H.: Predator-prey pigeon-inspired optimization for UAV three-dimensional path planning. Adv. Swarm Intell. **8795**, 96–105 (2014)
29. Benito, J., Mease, K.: Reachable and controllable sets for planetary entry and landing. J. Guid. Control Dyn. **33**(3), 641–654 (2010)
30. Bollino, K., Ross, I., Doman, D.: Six-degrees-of-freedom trajectory optimization for reusable launch vehicle footprint determination. Space Flight Mech. **130**(2), 859–878 (2008)
31. Phillips, T.H.: A common aero vehicle (CAV) model, description, and employment guide. Schafer Corporation for Air Force Research Laboratory (AFRL) and Air Force Space Command (AFSPC) (2003)